Journal of ELECTRONIC MATERIALS, Vol. 42, No. 6, 2013
DOI: 10.1007/s11664-013-2556-5

Investigation of the Properties of Ba-Substituted $La_{0.7}Sr_{0.3-x}Ba_xMnO_3$ Perovskite Manganite Films for Resistive Switching Applications

SUN GYU CHOI,[1] HONG-SUB LEE,[1] GEUN YOUNG YEOM,[2] and HYUNG-HO PARK[1,3]

1.—Department of Materials Science and Engineering, Yonsei University, Seoul 120-749, Korea. 2.—Department of Materials Science and Engineering, Sungkyunkwan University, Suwon, Kyunggi-do 440-746, Korea. 3.—e-mail: hhpark@yonsei.ac.kr

$La_{0.7}Sr_{0.3-x}Ba_xMnO_3$ (LSBMO: x = 0.09, 0.18, and 0.27) thin films were prepared on Pt-coated Si substrates using a radiofrequency magnetron sputtering technique at a substrate heating temperature of 450°C. The effects of varying the amount of substituted Ba^{2+} on the physical, chemical, and electrical properties of the perovskite manganite films were systematically investigated. X-ray diffraction showed that the growth orientation and crystallinity of films were not affected by the amount of substituted Ba cations. Raman spectroscopy was used to determine the tilt of MnO_6 octahedra and the Jahn–Teller-type distortion variation of the manganite films. The change in covalent characteristics of Mn–O bonds with increasing amounts of Ba^{2+} substituent was analyzed by x-ray photoelectron spectroscopy, specifically to examine the effects of bond characteristics on the resistive switching properties of LSBMO. The resistance of the LSBMO films increased with increasing Ba^{2+} content due to an increase in the covalent nature of Mn–O bonds. The resistive switching ratio increased with increasing Ba^{2+} amount, and relationships among resistive switching, Jahn–Teller distortion, and Mn–O bond character of LSBMO films were interpreted.

Key words: $La_{0.7}Sr_{0.3-x}Ba_xMnO_3$, Jahn–Teller distortion, XPS, Raman, resistive switching

INTRODUCTION

Resistive random-access memory (ReRAM) is a nonvolatile memory that can change its resistance between two reversible high- and low-resistance states with applied voltage pulses. ReRAM has garnered attention due to its simple metal–insulator–metal (MIM) structure, low power consumption, and fast operation speed.[1,2] Resistive switching behavior has been observed in various transition-metal oxides, such as mixed-valence perovskite manganites, especially with $Ln_{1-x}A_xMnO_3$ (where Ln are trivalent lanthanide cations and A are divalent alkaline-earth cations).[3] Perovskite manganite films exhibit bipolar resistive switching behavior without a "forming process," and thus can be understood in terms of an interface-type resistive switching model. In the case of interface-type resistive switching, a resistance change occurs at the interface between the metal electrodes and the oxide. Recent studies have demonstrated that, in the case of clockwise switching, redox between the reactive metal electrode and the resistive switching material in the vicinity of the interface is the main cause of interface-type resistive switching.[4–6] The reduction of interface regions of $Ln_{0.7}A_{0.3}MnO_3$ releases electrons, which can then occupy chemically doped holes in the Mn 3d $e_g^1 \uparrow$ band, resulting in increased resistance of the reduced region.[7]

The electrical and magnetic properties of perovskite manganite films are affected by lattice deformation

(Received June 29, 2012; accepted March 1, 2013; published online April 9, 2013)

resulting from differences in cation size. As the Ln and/or A ion size in $Ln_{1-x}A_xMnO_3$ increases, the lattice structure transforms from orthorhombic to rhombohedral and the Mn–O–Mn bond angle is straightened to 180°. This lattice distortion has a strong effect on the electrical conduction of perovskite manganite and is referred to as the double exchange theory, where the transport property and resistance of perovskite manganite depend on the number of Mn–O–Mn bonds, bond length, and bond angle.[8]

For resistive switching, when reactive metal electrodes are used, effective redox and electrochemical migration of oxygen ions should be induced. In this study, the tolerance factor of $La_{0.7}Sr_{0.3-x}Ba_xMnO_3$ (LSBMO) films was altered by substitution with Ba^{2+} cations to elucidate the effects of Mn–O covalent bond characteristics and Jahn–Teller effects on the resistive switching properties of films. Because Ba cations have more ionic bond characteristics and larger ionic size than Sr cations, they induce a change in Mn–O bonds and cause lattice distortion when Ba is substituted into a $La_{0.7}Sr_{0.3}MnO_3$ (LSMO) film. Mn–O octahedral distortion and Mn–O bond characteristics can affect the electrical resistivity of films, and structural distortion and Mn–O bonds can affect the electrochemical migration of oxygen ions, primarily the resistive switching ratio.

EXPERIMENTAL PROCEDURES

$La_{0.7}Sr_{0.3-x}Ba_xMnO_3$ (x = 0.09, 0.18, and 0.27) films were prepared on Pt(111)/Ti/SiO_2/Si(100) substrates by RF magnetron sputtering from a powder target. The $La_{0.7}Sr_{0.3-x}Ba_xMnO_3$ (x = 0.09, 0.18, and 0.27) target was prepared by a standard solid-state reaction method using La_2O_3, $SrCO_3$, $BaCO_3$, and Mn_2O_3 powders as starting materials. The working pressure was 5 mTorr during deposition. During the deposition of films, the substrate temperature was kept at 450°C and the Ar gas flow rate was maintained at 20 sccm. The thickness of the manganite films was approximately 250 nm. The Au (50 nm)/Al (150 nm) top electrode film was patterned onto the LSBMO films using a 200-μm-diameter metal shadow mask and an e-beam evaporator. The final sample structure was Au/Al/LSBMO/Pt(111)/Ti/SiO_2/Si(100).

The crystal structure of the films was analyzed by glancing-angle x-ray diffraction (GAXRD) using a Rigaku diffractometer with Cu K_α radiation and incident angle of 1°. Surface morphology was studied by atomic force microscopy (AFM) using an XE-100 (Park Systems) in noncontact mode. Raman measurements were conducted using a LabRam HR with the 514.532 nm line of an Ar laser for excitation. The chemical states and composition of the films were analyzed by x-ray photoelectron spectroscopy (XPS) using a K-alpha (Thermo VG) with a monochromated Al K_α radiation source ($h\nu$ = 1486.6 eV) and 50 eV pass energy. The sampling area was 400 μm in diameter, and information depth was approximately 3 nm. Current–voltage (I–V) characteristics were measured using an Agilent B1500A semiconductor device analyzer. Positive bias was defined as flow of current from the top to the bottom electrode. Current–voltage characteristics were measured by a voltage bias sweep as follows: 0 V → $-V_{max}$ (−4 V) → 0 V → $+V_{max}$ (4 V) → 0 V. All I–V measurements were taken at room temperature, and a compliance of 10 mA was applied to prevent breakdown of the MIM structure.

RESULTS AND DISCUSSION

Goldschmidt's tolerance factor (t) has been typically used as a basis for the formation of perovskite structures, and a number of researchers have used this tolerance factor to analyze perovskite stability.[9] An ideal perovskite structure has ABO_3 stoichiometry and cubic crystal structure, consisting of a three-dimensional framework of corner-sharing BO_6 octahedra. The A-site cation fills the 12 coordinate cavities formed by the BO_6 network and is surrounded by 12 equidistant anions.[10] Tolerance factors of $La_{0.7}Sr_{0.3-x}Ba_xMnO_3$ (x = 0.09, 0.18, and 0.27) were calculated as 0.993, 0.998, and 1.004, respectively, using the equation, $t = [r(O^{2-}) + r(La^{3+}) + r(A^{2+})]/2^{1/2}[r(O^{2-}) + r(Mn^{3+}) + r(Mn^{4+})]$.[11] The ionic radii of La^{3+}, Sr^{2+}, and Ba^{2+} for 12-coordination were 1.36 Å, 1.44 Å, and 1.61 Å, respectively, while those of Mn^{3+} and Mn^{4+} for 6-coordination were 0.645 Å and 0.530 Å, respectively. The O^{2-} radius was 1.34 Å.[12] With a tolerance factor of 1, the crystal structure of the film was ideal cubic in the absence of any compressive or tensile internal strain. These calculated values indicated that $La_{0.7}Sr_{0.12}Ba_{0.18}MnO_3$ had the most ideal cubic structure of the films tested.

Figure 1 shows GAXRD patterns of LSBMO thin films with different tolerance factors from 0.993 to 1.004. As shown in Fig. 1, LSBMO films deposited on Pt-coated silicon substrate showed polycrystalline and pseudocubic structures. Diffraction peaks corresponding to (100), (110), (111), (200), (222), (211), and (220) were seen in the LSBMO films. Generally, LSMO and $La_{0.7}Ba_{0.3}MnO_3$ films exhibit rhombohedral structures.[13] Substitution of Sr with Ba in LSMO did not result in a structural change. Likewise, as shown by the patterns, the $La_{0.7}Sr_{0.12}Ba_{0.18}MnO_3$ film had the most intense diffraction peaks, and the highly crystalline state was tentatively attributed to an ideal tolerance factor of 0.998.

The surface morphology of the LSBMO films was studied by AFM analysis in noncontact mode, as shown in Fig. 2. The root-mean-square (RMS) roughness of $La_{0.7}Sr_{0.21}Ba_{0.09}MnO_3$, $La_{0.7}Sr_{0.12}Ba_{0.18}MnO_3$, and $La_{0.7}Sr_{0.03}Ba_{0.27}MnO_3$ were 2.939 nm, 2.962 nm, and 2.697 nm, respectively. The almost uniform values of RMS roughness were a result of small variations in the tolerance factor, with

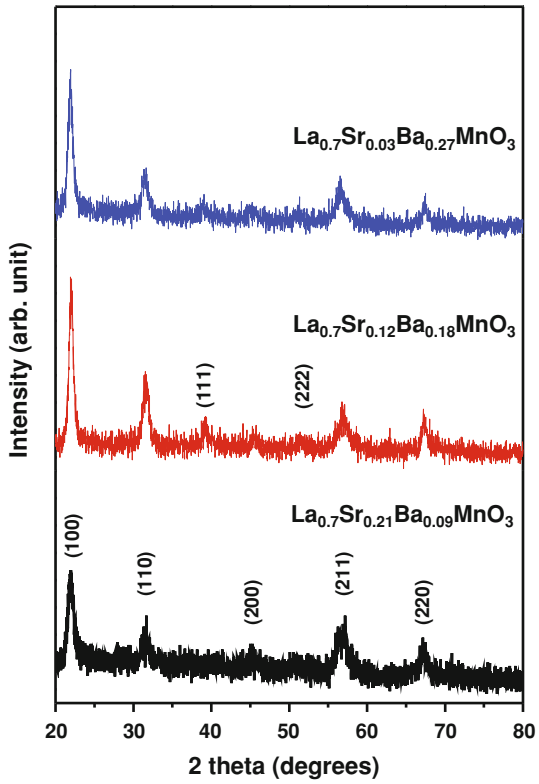

Fig. 1. XRD patterns of $La_{0.7}Sr_{0.3-x}Ba_xMnO_3$ (x = 0.09, 0.18, and 0.27) films.

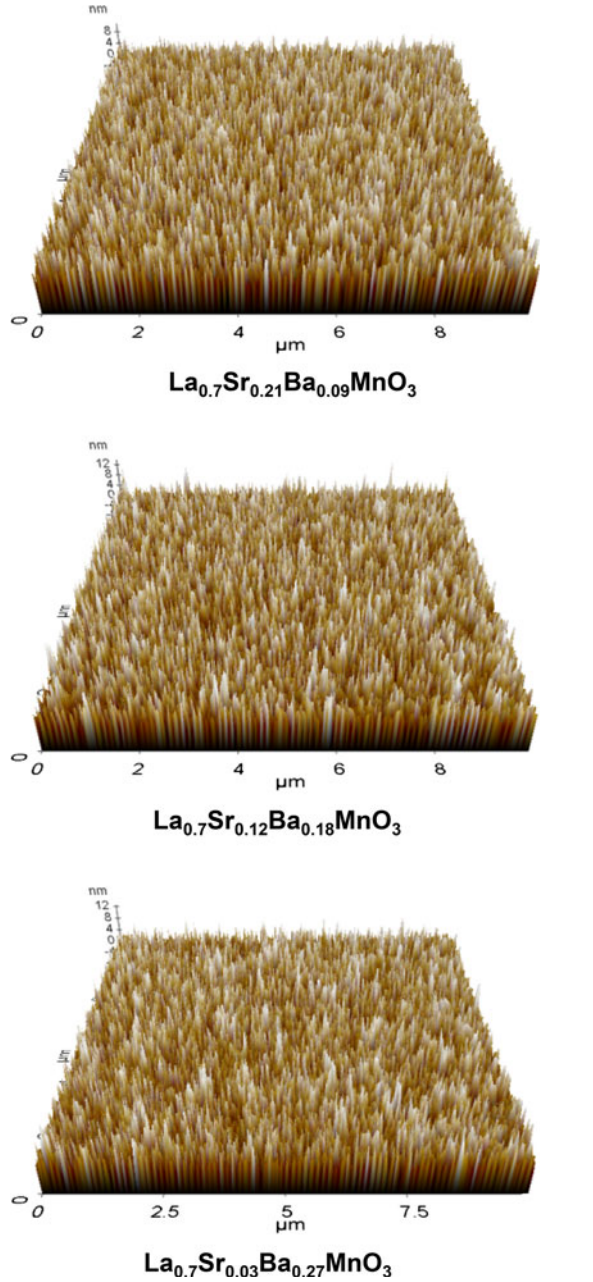

Fig. 2. AFM surface morphology of $La_{0.7}Sr_{0.3-x}Ba_xMnO_3$ (x = 0.09, 0.18, and 0.27) films.

the most ideal being $La_{0.7}Sr_{0.12}Ba_{0.18}MnO_3$. However, the RMS value of $La_{0.7}Sr_{0.12}Ba_{0.18}MnO_3$ may have also been related to an ideal tolerance factor inducing the highly crystalline state.

Figure 3 shows Raman spectra of LSBMO films, where the three main peaks correspond to the following modes and symmetries: $A_g(2)$ y-rotation mode, $A_g(3)$ bending mode, and $B_{2g}(1)$ stretching mode at 190 cm^{-1} to 245 cm^{-1}, 470 cm^{-1} to 500 cm^{-1}, and 610 cm^{-1} to 630 cm^{-1}, respectively.[14–16] The observed frequency shift at approximately 220 cm^{-1} was due to variations in the divalent cation size. The Raman peak at 220 cm^{-1} for $La_{0.7}Sr_{0.21}Ba_{0.09}MnO_3$ shifted to 208 cm^{-1} and 213 cm^{-1} as the Ba stoichiometry increased to 0.18 and 0.27, respectively, which was attributed to a change in tolerance factor. Specifically, when the Ba substitution increased from 0.09 to 0.27, the average ionic radius of the A cation site in the ABO_3 perovskite structure increased from 1.3993 Å to 1.4299 Å. As the tolerance factor increased to 1, the Raman peak indicated that the tilt of the MnO_6 octahedron moved to low wavenumber, suggesting that the orthorhombic octahedral distortion was compensated by the large size of the cation substitution.[17] As more Ba cation was substituted into the LSBMO structure, as in the case of the 0.27 condition, the tolerance factor increased to larger than 1, until rhombohedral distortion was finally generated. Thus, the Raman peak shifted to a slightly higher wavenumber, 213 cm^{-1}.[18] Out-of-phase Mn–O bending of the $A_g(3)$ shift was also observed, with the same shift tendency as the tilt of the MnO_6 octahedron. The in-phase stretching of $B_{2g}(1)$ at 635 cm^{-1} failed to show any noticeable deviation, because the symmetric stretching of basal oxygen was incoherent with the tolerance factor variation.[19] From the Raman spectral analysis of the Ba-substituted samples, octahedral distortion was minimized in $La_{0.7}Sr_{0.12}Ba_{0.18}MnO_3$ films.

The composition of the films was obtained using XPS, the results of which are presented in Table I. The measured composition was almost the same as the target value. To investigate the chemical bond state change according to the Ba substituent amount in LSBMO, Mn 2p XPS spectra were obtained. Figure 4 shows the Mn 2p spectra of different trivalent cation sizes in $La_{0.7}Sr_{0.3-x}Ba_xMnO_3$ (x = 0.09, 0.18, and 0.27) films. The Mn $2p_{3/2}$ binding energy shifted from 641.6 eV to 641.3 eV as the Ba cation substitution increased from 0.09 to 0.27. Because the Mn valence was not changed, the Mn $2p_{3/2}$ chemical shift of the LSBMO films could be explained by a change in the Mn–O bond characteristics. Specifically, the Mn–O bond is thought to become more covalent when Sr^{2+} is substituted by Ba^{2+}, especially as the electronegativities of Sr and Ba are 0.95 and 0.89, respectively.[20] The Mn–O bond in Mn–O–Ba is more covalent than the Mn–O bond in Mn–O–Sr because of the more ionic bond characteristics of Ba–O compared with Sr–O. This increase of the covalent nature of Mn–O bonds could induce an increase of LSBMO resistance because the principal electron transport mechanism in perovskite manganite is a double exchange mechanism in Mn^{3+}–O^{2-}–Mn^{4+} chains.[8]

Figure 5 shows the I–V characteristics of Au/Al/LSBMO/Pt structures when the maximum positive and negative voltage bias was fixed at 4 V. The applied negative bias voltage produced a low-resistance state (LRS), where the resistance decreased as the negative voltage increased. In the positive bias voltage region, a high-resistance state (HRS) was achieved. Figure 5 shows the interface-type bipolar switching behavior of clockwise switching.[21] This clockwise resistive switching behavior without a forming process was attributed to "interface-type switching" as a redox state between LSBMO and the reactive Al top electrode.[6] Upon applying a positive bias voltage to LSBMO films, the film just beneath the Al electrode was reduced through the oxidation of the Al top electrode by electrochemical migration of oxygen ions. An oxygen-deficient layer was formed at the top interface region of the LSBMO film, and the HRS was induced because oxygen vacancies generate electron carriers that erase hole carriers in p-type perovskite manganite.[22–24] Conversely, a negative bias voltage recovered the reduced LSBMO films by oxidation (the negative voltage pushes out oxygen ions from the interfacially oxidized Al electrode to the reduced LSBMO), thereby lowering the resistivity to the LRS.[25] Our observation of a decrease in the resistance of LSBMO films with increasing Ba substituent content agrees well with our XPS results (Fig. 4), which showed increased covalent characteristics of Mn–O bonds with increasing Ba substitution content.

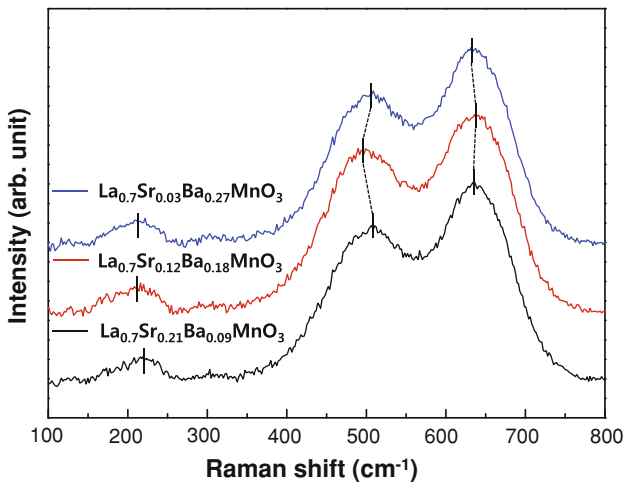

Fig. 3. Raman spectra of $La_{0.7}Sr_{0.3-x}Ba_xMnO_3$ (x = 0.09, 0.18, and 0.27) films.

To further analyze the resistive switching properties, the resistive switching (RS) ratio was calculated as (HRS – LRS)/LRS.[26] HRS and LRS values of –1 V/+1 V were used for the RS ratio calculation of $La_{0.7}Sr_{0.21}Ba_{0.09}MnO_3$, $La_{0.7}Sr_{0.12}Ba_{0.18}MnO_3$, and $La_{0.7}Sr_{0.03}Ba_{0.27}MnO_3$ films, and the results were 62/37, 205/44, and 277/41, respectively. The switching ratio and resistance of films increased with increasing Ba substitution content. Specifically, $La_{0.7}Sr_{0.21}Ba_{0.09}MnO_3$ and $La_{0.7}Sr_{0.03}Ba_{0.27}MnO_3$ films exhibited smaller negative operating voltage compared with $La_{0.7}Sr_{0.12}Ba_{0.18}MnO_3$ film. The octahedral distortion was confirmed for $La_{0.7}Sr_{0.21}Ba_{0.09}MnO_3$ and $La_{0.7}Sr_{0.03}Ba_{0.27}MnO_3$ by the Raman observations, and in general, increased structural distortion appeared to be a favorable condition for ion migration.[27] Therefore, it can be said that, for the LSBMO samples within the compositional range of this study, structural distortion affected the electrochemical migration of oxygen ions, i.e., operating voltage and resistance. Furthermore, an enhancement in the Mn–O covalent character also induced an increase in the resistance of

Table I. Composition data of $La_{0.7}Sr_{0.3-x}Ba_xMnO_3$ (x = 0.09, 0.18, and 0.27) films from XPS measurements (at.%)

	La	Sr	Ba	Mn	O
$La_{0.7}Sr_{0.21}Ba_{0.09}MnO_3$	14.6 ± 0.1	4.9 ± 0.1	2.3 ± 0.1	18.0 ± 0.1	60.2 ± 0.1
$La_{0.7}Sr_{0.12}Ba_{0.18}MnO_3$	14.6 ± 0.1	2.9 ± 0.1	4.5 ± 0.1	18.0 ± 0.1	60.0 ± 0.1
$La_{0.7}Sr_{0.03}Ba_{0.27}MnO_3$	14.4 ± 0.1	0.6 ± 0.1	6.5 ± 0.1	18.0 ± 0.1	60.5 ± 0.1

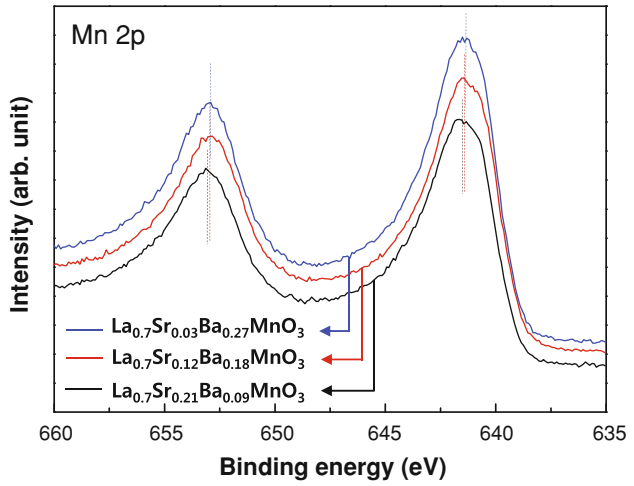

Fig. 4. Mn 2p XPS spectra of $La_{0.7}Sr_{0.3-x}Ba_xMnO_3$ (x = 0.09, 0.18, and 0.27) films.

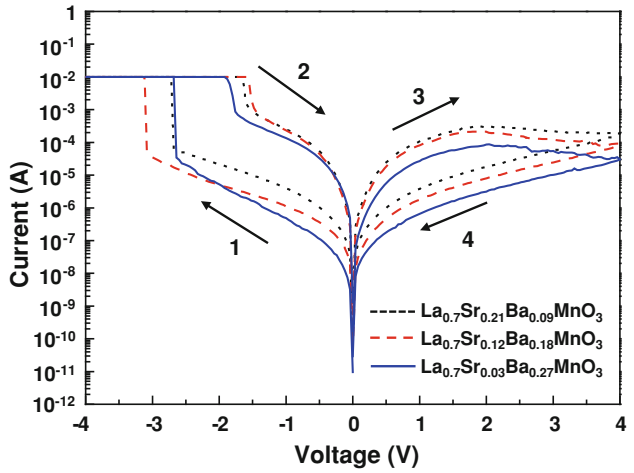

Fig. 5. Resistive switching I–V curves of Au/Al/$La_{0.7}Sr_{0.3-x}Ba_xMnO_3$ (x = 0.09, 0.18, and 0.27)/Pt MIM structures.

films (both LRS and HRS), however this was more important for the HRS, because the effect could be maximized with a limited number of charge carriers. As a result, an increase in switching ratio was observed with increasing Ba substitution content.

Based on the above observations, it can be said that the reversible resistive switching phenomenon including resistance, operating voltage, and switching ratio of the perovskite manganite family can be controlled by substitution of A-site cations to modify structural distortions and Mn–O bond characteristics.

CONCLUSIONS

The tolerance factors of polycrystalline $La_{0.7}Sr_{0.3-x}Ba_xMnO_3$ (x = 0.09, 0.18, and 0.27) films were controlled by Ba cation substitution. An increase in covalent Mn–O bond characteristics with increasing Ba substituent was confirmed via observation of a Mn 2p binding energy shift. Increased resistance and switching ratios of LSBMO films were observed with increasing Ba substitution content, which was due to an increase of the covalent nature of Mn–O bonds. In addition, an increase in the structural distortion from the change in the tolerance factor (t) led to a decrease in the operating voltage due to a favorable condition for oxygen ion migration. From these results, we conclude that substitution of Sr with Ba in $La_{0.7}Sr_{0.3}MnO_3$ films strongly affected Mn–O bonds, resistance, and Jahn–Teller distortion of MnO_6 octahedrons, which control the resistive switching properties of perovskite manganite films.

ACKNOWLEDGEMENTS

This work was supported by the Industrial Strategic Technology Development Program (10041926, Development of high density plasma technologies for thin film deposition of nanoscale semiconductor and flexible display processing) funded by the Ministry of Knowledge Economy (MKE, Korea).Experiments at PLS were supported in part by MEST and POSTECH.

REFERENCES

1. X.J. Liu, X.M. Li, Q. Wang, R. Yang, X. Cao, W.D. Yu, and L.D. Chen, *Phys. Status Solidi A* 207, 1204 (2010).
2. S.-L. Li, Z.L. Liao, J. Li, J.L. Gang, and D.N. Zheng, *J. Phys. D Appl. Phys.* 42, 045411 (2009).
3. S.T. Hsu, T. Li, and N. Awaya, *J. Appl. Phys.* 101, 024517 (2007).
4. D.J. Seong, M. Hassan, H. Choi, J. Lee, J. Yoon, J.B. Park, W. Lee, M.S. Oh, and H. Hwang, *IEEE Electron Device Lett.* 30, 919 (2009).
5. Y.B. Nian, J. Strozier, N.J. Wu, X. Chen, and A. Ignatiev, *Phys. Rev. Lett.* 98, 146403 (2007).
6. K. Szot, W. Speier, G. Bihlmayer, and R. Waser, *Nat. Mater.* 5, 312 (2006).
7. S.G. Choi, H.-S. Lee, H.J. Choi, S.-W. Chung, and H.-H. Park, *J. Phys. D Appl. Phys.* 44, 422001 (2011).
8. J.-S. Fang, F.-W. Tsai, and T.-S. Chin, *Jpn. J. Appl. Phys.* 41, 600 (2002).
9. V.M. Goldschmidt, *Ber. Dtsch. Chem. Ges.* 60, 1263 (1927).
10. C. Li, K.C.K. Soh, and P. Wu, *J. Alloy Compd.* 372, 40 (2004).
11. V.M. Goldschmidt, *Naturwissenschaften* 14, 477 (1926).
12. S.V. Trukhanov, *J. Exp. Theor. Phys.* 100, 95 (2005).
13. A.P. Ramirez, *J. Phys. Condens. Matter* 9, 8187 (1997).
14. M.N. Iliev and M.V. Abrashev, *J. Raman Spectrosc.* 32, 805 (2001).
15. V.A. Amelitchev, B. Güttler, O.Y. Gorbenko, A.R. Kaul, A.A. Bosak, and A.Y. Ganin, *Phys. Rev. B* 63, 104430 (2001).
16. M.N. Iliev, M.V. Abrashev, H.-G. Lee, V.N. Popov, Y.Y. Sun, C. Thomsen, R.L. Meng, and C.W. Chu, *Phys. Rev. B* 57, 2872 (1998).
17. B. Güttler, V.A. Amelitchev, O.Y. Gorbenko, and A.R. Kaul, *Phase Transit.* 76, 63 (2003).
18. M.N. Iliev, M.V. Abrashev, J. Laverdière, S. Jandl, M.M. Gospodinov, Y.-Q. Wang, and Y.-Y. Sun, *Phys. Rev. B* 73, 064302 (2006).
19. A.E. Pantoja, H.J. Trodahl, R.G. Buckley, Y. Tomioka, and Y. Tokura, *J. Phys. Condens. Matter* 13, 3741 (2001).
20. S.G. Choi, S.-J. Wang, H.H. Park, M. Hong, and K.-H. Kwon, *J. Vac. Sci. Technol. A* 28, 1 (2010).
21. C.J. Kim and I.W. Chen, *Thin Solid Films* 515, 2726 (2006).
22. A. Sawa, *Mater. Today* 11, 28 (2008).
23. S.-L. Li, D.S. Shang, J. Li, J.L. Gang, and D.N. Zheng, *J. Appl. Phys.* 105, 033710 (2009).

24. S. Asanuma and H. Akoh, *Phys. Rev. B* 80, 235113 (2009).
25. M. Hasan, R. Dong, H. Choi, J. Yoon, J.-B. Park, D.-J. Seong, and H. Hwang, *J. Electrochem. Soc.* 156, H239 (2009).
26. K. Tsubouchi, I. Ohkubo, H. Kumigashira, M. Oshima, Y. Matsumoto, K. Itaka, T. Ohnishi, M. Lippmaa, and H. Koinuma, *Adv. Mater.* 19, 1711 (2007).
27. A. Kushima and B. Yildiz, *J. Mater. Chem.* 20, 4809 (2010).